SERI/TP-252-2332
UC Category: 64
DE84013028

An Experimental Study of Steam Condensation on Water in Countercurrent Flow in Presence of Inert Gases

D. Bharathan
J. Althof

August 1984

To be presented at the ASME
Winter Annual Meeting
New Orleans, Louisiana
December 1984

Prepared under Task No. 4001.21
FTP No. 457

Solar Energy Research Institute
A Division of Midwest Research Institute

1617 Cole Boulevard
Golden, Colorado 80401

Prepared for the
U.S. Department of Energy
Contract No. DE-AC02-83CH10093

Printed in the United States of America
Available from:
National Technical Information Service
U.S. Department of Commerce
5285 Port Royal Road
Springfield, VA 22161
Price:
Microfiche A01
Printed Copy A02

AN EXPERIMENTAL STUDY OF STEAM CONDENSATION ON WATER IN COUNTERCURRENT FLOW IN PRESENCE OF INERT GASES

D. Bharathan*
J. Althof*

Solar Energy Research Institute
1617 Cole Boulevard
Golden, Colorado 80401

ABSTRACT

Experimental results of investigating steam condensation on water in the presence of (noncondensable) inert gases at low temperatures and pressures relevant to open-cycle ocean thermal energy conversion (OTEC) systems are reported. Seven different condenser configurations were tested. The experimental data are correlated using a liquid flow fraction and a vent fraction to yield simple relationships of condenser performance over a wide range of test conditions. Performance maps and envelopes are provided for evaluating the relative merits of tested configurations. The height of transfer unit (HTU) for condensation ranges from 0.2 to 0.3 m among the various condenser geometries. Also reported are the pressure-loss coefficients for all the tested geometries.

NOMENCLATURE

A	cross-sectioned area of the condenser (m^2)
a_p	packing surface area to volume (m^2/m^3)
a_w/a_t	wetted to total area ratio
C	heat capacity ratio
C_{pl}	specific heat of liquid (kJ/kg K)
C_{pv}	specific heat of vapor (kJ/kg K)
C_{pw}	specific heat of water (kJ/kg K)
D_c	outer diameter of the condenser (m)
d_p	packing characteristic diameter (m)
G	condenser gas loading (kg/s m^2)
H	nondimensional packing height
h	condenser heat load (kW)
h_{fg}	latent heat of condensation (kJ/kg)
HTU	condensation height of transfer unit (m)
Ja	Jacob number
K	condenser pressure-loss coefficient
L	condenser liquid loading (kg/s m^2)
l_c	height of the condenser contacting region (m)
l	liquid flow fraction
M	molecular weight
$\dot{m}$	mass flow rate (kg/s)
NTU	condenser number of transfer units
P_c	condenser inlet pressure (Pa)
Δp	pressure loss (Pa)
$\dot{Q}$	volumetric vent rate (m^3/s)
q	steam dynamic pressure (Pa)
R	universal gas constant (kJ/kg mol K)
St	Stanton number
T	temperature (K)
ΔT	driving temperature differential (K)
U_v	volumetric heat transfer coefficient (kW/m^3 K)
v	vent fraction
x	inert gas mass fraction
y	inert gas mole fraction

Greek

ε	condensation effectiveness
ξ	fractional steam effectiveness
ρ	gas density (kg/m^3)

Subscripts

a	average liquid

*Member ASME

c	condensed
e	exit
exp	experimental
i	inert, inlet
id	ideal
ℓ	liquid
max	maximum
min	minimum
o	outlet
s	steam
sat	saturation
v	vapor
w	water

INTRODUCTION

Direct-contact heat transfer is an area of current research interest for several reasons. First, the heat exchange surfaces are a major expense of the total system and are subject to corrosion and fouling and need maintenance. Further, using a solid surface to transfer heat from two fluids requires a significant temperature difference, which resul in a loss of overall system efficiency. Examples of such situations can be found in geothermal systems, in ocean thermal energy conversion systems, in bottoming cycles for power plants situated near low-temperature sinks, solar ponds, and energy systems in which the available temperature difference is small. As high quality energy becomes more expensive and less available, techniques that enhance the heat transfer efficiency and reduce the deterioration in the energy quality available for doing productive work are becoming increasingly more important.

This paper reports on one aspect of direct-contact heat transfer problems, namely the heat and mass transfer between two streams of the same fluid in which the vapor condenses in direct contact with its own liquid.

Specifically, condensing steam on water at low pressures in the presence of (noncondensable) inert gases is studied. The presence of inert gases is known to deteriorate the condenser performance and operating cost three ways: by increasing the condenser operating pressure, increasing the gas-side resistance to mass transfer across the gas-liquid interface, and requiring exhaust compressors for continuous removal of the inert gases.

At the maximum potential performance of a condenser configuration, the operation of the condenser may be limited by the condensation rates (or the heat-transfer rates) within the condenser or the exhaust pumping capacity (nominally expressed as a volumetric flow rate) of the gas exhaust system or both. In fact, these two limitations are related. Poor heat transfer in the condenser will dictate large exhaust capacities, and an inadequate exhaust system will deteriorate the condensation heat transfer.

Presence of inert gases is a significant problem in almost all types of condensers, including power condensers. This problem is considerably larger in OTEC systems using the open- or Claude-cycle approach (1). The level of inert gases desorbed from the seawater streams imposes a significant burden on the condensation process and requires continuous exhaust pumping.

This study identifies condenser configurations that can increase condensation efficiencies and decrease the amount of exhaust pumping power needed to remove inert gases from the condenser area. It also describes an experimental investigation of the relative merits of various configurations. The scope of the study is limited to studying steam condensation in direct contact with water at temperatures and pressures relevant to open-cycle OTEC systems. Seven different countercurrent condenser geometries were studied. The experimental variables include steam mass flow rate, water flow rate, inert gas content in steam, and a volumetric exhaust flow rate.

Experimental results are presented as steam-side and water-side effectiveness and steam pressure loss through the condenser as functions of a liquid flow fraction and a vent fraction. Limitations posed by condensation (heat-transfer) rates and the vacuum exhaust capacity for all the seven configurations are identified in a performance map of water and steam effectiveness. Relative merits of the various configurations can be identified through performance maps of parasitic power and cost for a typical open-cycle OTEC application.

Suitable liquid loadings for countercurrent condensation are in the range of 20 to 40 kg/s m^2 based on pressure loss considerations. For the best condenser configuration at optimum steam and water effectiveness the condensation HTU ranged from 0.2 to 0.35 m. The pressure losses between the different configurations varied widely over an order of magnitude.

BACKGROUND

Heat Transfer

Literature in the area of direct-contact condensation (DCC) is scant. Comprehensive treatments of suitable designs and analyses of industrial and power systems, such as those available for surface condensers, are not available. Sideman and Moalem-Maron (2) provide a brief review of the majority of earlier works on this subject. Since DCC depends strongly on the geometry of the vapor-liquid interface, they categorize the earlier works according to the available interface, such as free-liquid interfaces (including jets, films, and drops), bubble columns, and other contacting devices (packed beds and baffle trays). Among some hundred works cited, we found the works of Wilke et al. (3), Cheng (4), and Thomas et al. (5) of particular interest to this study. Wilke (3) reported Cheng's (4) experimental data on steam condensation in countercurrent flow with Aroclor as the coolant in 60- and 90-cm-high, 3-cm-diameter, packed columns with 2.5-cm Raschig rings. The condensation was primarily controlled by the liquid-side resistance. Measured HTU varied from 24 to 46 cm for liquid loadings of 20 to 40 kg/s m^2.

Thomas et al. (5) studied condensation of Freon R-113 on water in a 15-cm (outside diameter), 122-cm-high column packed with 3.2-cm diameter ceramic spheres and 2.5-cm-ceramic Berl saddles. Their data, along with Cheng's (4) data, were correlated by a Stanton Number,

$$St = \frac{U_v}{(\dot{m}_v/A)\, C_{pv}\, a_p\, (a_w/a_t)} = 0.14\, Ja\, C^{-0.21_H - 0.67} . \quad (1)$$

Here the Jacob number Ja is defined as

$$Ja = \frac{h_{fg}}{C_{pv}\,(T_{sat} - T_a)} \quad (2)$$

where

T_{sat} = the vapor saturation temperature

T_a = the average temperature of the liquid in the packed column.

A heat capacity ratio C is defined as

$$C = \frac{\dot{m}_l \, C_{pl}}{\dot{m}_v \, C_{pv}} . \qquad (3)$$

The variable H represents the packing height made dimensionless by the characteristic packing diameter d_p.

A review of available literature on process direct-contact heat exchange is provided by Fair (6-8). He summarizes available correlations for gas and liquid-side heat transfer coefficients for various types of contactors including packed beds, baffle trays, spray columns, cross-flow columns, and pipe line contactors. His analyses and design methods, however, are limited to conditions where the sensible and the latent heat loads are of nearly equal magnitude. Little data are included for conditions where the latent load is the major heat duty of the contactor.

Flooding and Pressure Drop Considerations

The countercurrent geometry for this condensation study was chosen to achieve a maximum possible concentration of inert gases as they exit the condenser. However, countercurrent geometries are prone to the flooding phenomenon, when the gas and liquid loadings through a packed column limit each other. For mass-transfer applications in packed columns Ref. 10 has a generalized correlation of flooding limits proposed by Sherwood et al. (9). Typical liquid loadings associated with mass-transfer applications range from 60% to 80% of the flooding limits with, approximately 90 kg/s m^2 as an upper limit.

For a direct-contact condenser, however, the HTU for condensation ranges from 0.2 to 0.4 m. Typically, the liquid free-fall space at the bottom of the packing is approximately 1 HTU. Considerable condensation may occur in this space, causing a significant reduction in the vapor loading at the bottom of the packing. Thus, estimated flooding limits based on mass-transfer applications may prove to be overly conservative for a direct-contact condenser. Usually, an upper limit of allowable pressure loss through the condenser would limit the gas and liquid loadings for condenser applications.

EXPERIMENTAL APPARATUS

The heat and mass transfer laboratory of the Solar Energy Research Institute (SERI) is designed to study and improve methods of transferring heat and mass under the small driving forces that often exist when the sun is the energy source for the process. The near-term objective of the laboratory research is to investigate the heat and mass transfer phenomena relevant to various open-cycle OTEC systems.

The experimental apparatus, shown in Fig. 1, consists of a test cell that houses the evaporator and the condenser, and warm and cold water loops that supply heat to and from the water jets. The warm water loop consists of a pump with a bypass, a heat exchanger with a bypass, a static mixer, a turbine flow meter, and a spout evaporator. A valve upstream of the heat exchanger regulates the warm water flow rate from 7 to 40 kg/s. The heat exchanger is supplied with hot water from a boiler with a variable heating range of 50 to 300 kW. The cold water loop is similar to the warm water loop except that the water is piped directly to a chiller. Falling streams of cold water through the countercurrent condenser condense the vapor generated in the evaporator. Since both loops are closed, an interconnecting line between the loops replenishes from

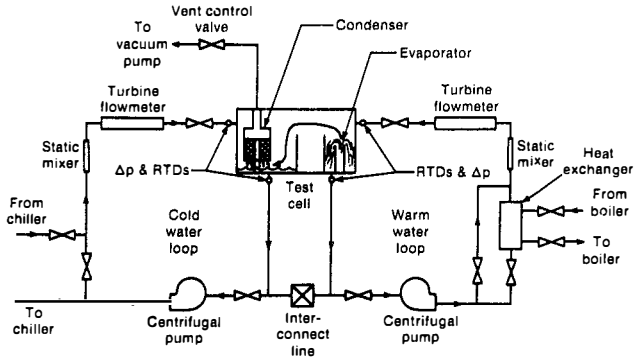

Fig. 1 Schematic of the Experimental Apparatus.

cold to warm loop the amount of water lost during evaporation.

The test cell is a horizontal, 1.5-m-diameter, 1.8-m-long cylinder. Reservoirs underneath the evaporator and the condenser sections allow separate collection of warm and cold water. Glass ports on the top and side provide for lighting, viewing, and photography.

The cell is evacuated by a three-stage gas exhaust system, consisting of a lobe-type blower, an oil-sealed compressor, and a liquid-ring vacuum pump. Nominal venting capacity of the exhaust system is 0.56 m^3/s. During tests, a butterfly valve located in the gas exhaust line controls the actual vent capacity. A threshold pressure of 700 Pa can be attained in the cell. At operating conditions the air leakage into the cell is nominally less than 1 mg/s. Additional details of the apparatus may be found in Green et al. (11).

A typical countercurrent condenser module was designed as shown in Fig. 2. Seven different condenser geometries were tested. The primary and common features of all the geometries were:

- A central 12.7-cm (inside diameter), plastic (PVC) water feed pipe
- A cylindrical enclosure to confine steam entry to the bottom annular opening around the condenser module
- A central 15.2-cm (inside diameter) pipe to exhaust uncondensed steam and inert gases from above the condenser module.

The relevant dimensions and features of each of the tested geometries is summarized in Table 1. The water distributor plate, when used, was located about 25-mm below the top of the water feed pipe. This plate was a 0.61-m-diameter plastic (Plexiglas®) plate with 9.5-mm perforations on a square pitch of 25 mm, with six 7-cm-long and 7-cm (inside diameter) plastic tubes inserted for vapor escape. The vapor escape space above was nominally 20 cm long for all cases.

INSTRUMENTATION AND UNCERTAINTIES

Typical temperature and pressure measurement locations around the countercurrent condenser module are also shown in Fig. 2.

Temperature in the liquid streams is measured with platinum resistance temperature detectors. The detector for measuring the condenser water inlet temperature T_{wi} was located in the water inlet pipe. The water outlet temperature T_{wo} was measured nearly 3 m downstream in the drain pipe to ensure uniformity in the bulk temperature distribution.

Steam inlet and outlet temperatures, T_{si} and T_{so}, respectively, were measured using wet-bulb detectors blanketed with cotton wicks wetted from a small water reservoir.

Table 1. Summary of Seven Tested Condenser Configurations

Configuration Number	Description	Length l_c (m)	Diameter D_c (m)	Remarks
1	Spiral Screen	0.6096	0.4572	First tested configuration; screens were perforated metal with 4.7 mm diameter holes at a triangular pitch of 6.4 mm. The spiral was a triple lead screw with a pitch of 20 cm. No water distributor plate was used here.
2	Three Baffles	0.5842	0.6096	The baffles were disc-donut type, with the disc or the donut providing a steam flow path blockage of 50%. The distance between baffles was nominally 20 cm.
3	Two Baffles	0.5842	0.6096	Same as in 2, except the bottom pair of disc and donut was removed.
4	One Baffle	0.5842	0.6096	Same as in 2, except the bottom two pairs of disc and donut were removed.
5	Spiral Rubber Mat	0.7842	0.6096	Similar to 1, but a spiral rubber screen with 7.1-mm-diameter holes at a pitch of 10.7 mm was used to ease fabrication. The spiral consisted of six lead screws with a pitch of 60 cm. A distributor plate was used here.
6	Munters Pack 27060	0.8128	0.6096	Commercially available cooling-tower fills, made of polyethylene (Munter's trade product PLASdek 27060). Surface area ratio a_p = 98 m^2/m^3.
7	Munters Pack 19060	0.8128	0.6096	Same as in 6 with Munter's trade product (PLASdek 19060). Surface area ratio a_p = 138 m^2/m^3.

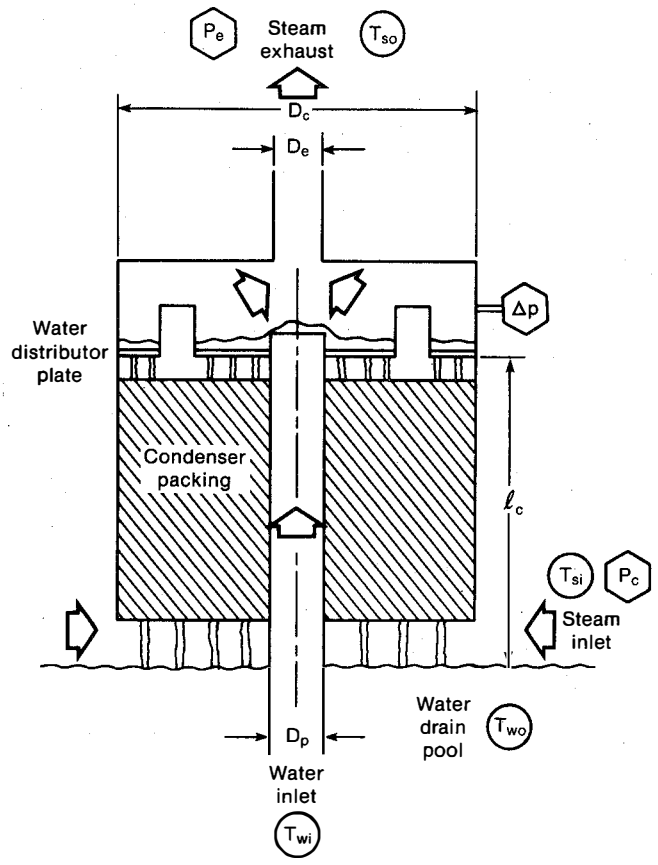

Fig. 2 Cross-sectional View of the Condenser Showing Details.

The pressure measurements include the condenser pressure P_c, a pressure loss across the condensing region Δp, and the exhaust pressure P_e.

Similar instrumentation is provided on the warm water side to evaluate the evaporation rates and an overall heat balance of the test loop.

Warm and cold water flow rates are measured using two turbine meters, each connected to a separate flow rate indicator and a frequency counter.

Inert gas injected into the test chamber was compressed air from the building air supply. The gas flow rate was monitored and controlled using two gas mass flow controllers (TYLAN, model FC-262).

The exhaust gas volumetric venting rate was measured by monitoring the absolute pressure and temperature of the exhaust stream just upstream of the exhaust compressor and by using a previously calibrated volumetric venting capacity of the compressor as a function of the compressor inlet pressure.

Detector resistances, pressure transducer voltages, flow meter pulses, and gas flow controller outputs were scanned through a data acquisition and control unit controlled by a desk-top computer (Hewlett-Packard Model 9845A). At each test condition ten samples of each measurement were collected, and an average was stored on a magnetic tape for later data processing and analyses.

Temperatures throughout the system were monitored continuously to ensure steady-state operation during condenser tests.

Uncertainties in liquid and vapor temperatures arise from calibration errors in the detector probe, self-heating of the probe, stem conduction through the support elements, background radiation, and random errors in reading. The uncertainties in the inlet and outlet liquid temperatures are estimated to be ±0.015 K. Uncertainty in the vapor temperature measurements are estimated to be ±0.02 K.

Uncertainties in the liquid flow rate measurements arising from calibration errors in the flow meter and from random errors in reading are estimated to be

±0.14 kg/s. Uncertainty in the inert gas injection rate is estimated to be less than ±0.5% of the reading.

Based on random error propagation analyses for a typical experimental condition (200 kW heat flux, 10 kg/s cold water flow rate, 2 g/s inert gas flow rate, and a 0.20 m^3/s exhaust vent rate), the estimated uncertainties in the reported water and steam effectiveness are ±0.005 and ±0.010, respectively. Uncertainties in the reported pressure loss and the volumetric vent rate are estimated to be ±8%.

DATA ANALYSES

At every test condition, the raw experimental data obtained include the following measurements:

T_{si}	steam inlet temperature (K)
T_{so}	steam outlet temperature (K)
T_{wi}	water inlet temperature (K)
T_{wo}	water outlet temperature (K)
$\dot{m}_{wi}$	water inlet flow rate (kg/s)
$\dot{m}_{ii}$	inert gas inlet injection rate (kg/s)
$P_{c\ exp}$	condenser pressure at inlet (Pa)
Δp	pressure loss across the condenser (Pa)
$Q_{o\ exp}$	steam and inert volumetric vent rate at condenser exit (m^3/s).

For presentation of the experimental results, the data are processed as follows.

The following assumptions are made with respect to all calculations:

- The sensible heat content of the inert gas and steam is, in general, small compared with the latent heat of steam (typically less than 0.5%) and can be ignored in the calculations.
- The condensate flow rate is again small compared to the coolant water flow rate (typically less than 2%) and can be ignored.
- The average value for both the latent heat of condensation h_{fg} and the specific heat of water C_{pw} are adopted as 2470 kJ/kg K and 4.186 kJ/kg K, respectively.

The experimentally measured condenser pressure $P_{c\ exp}$ is verified by an iterative calculation for the theoretical pressure P_c and was found to agree within ±2% for all test conditions.

A theoretically required vent rate Q_o is calculated based on the inert gas flow rate and its exit density ρ_{io} and compared with the experimental value $Q_{o\ exp}$ and found to agree within ±10% for all the test conditions. Most of the data indicate that the experimental value is approximately 10% higher than Q_o.

The water and steam effectiveness, ε_w and ε_s, are defined as

$$\varepsilon_w = \frac{T_{wo} - T_{wi}}{T_{si} - T_{wi}} \tag{4}$$

and

$$\varepsilon_s = \frac{T_{si} - T_{so}}{T_{si} - T_{wi}} , \tag{5}$$

respectively. The water effectiveness ε_w provides a measure of the water temperature rise as it relates to the overall available driving temperature difference, whereas, the steam effectiveness relates to the temperature (partial pressure) decrease in steam at the condenser exit and, thus, provides a measure for the concentration of the inert gases.

Ideal Condenser

For data reduction an ideal case is defined as when the condenser attains equilibrium conditions at the inlet and outlet; i.e., $\varepsilon_s = \varepsilon_w = 1$; however, a finite pressure loss may occur through the condenser.

For the ideal case, the exit density of the inert gas can now be calculated as

$$\rho_{iid} = \frac{[P_c - P_{sat}(T_{wi}) - \Delta p]\ M_i}{R\ T_{wi}} . \tag{6}$$

The ideal vent rate for the case is

$$Q_{id} = \dot{m}_{ii}/\rho_{iid} . \tag{7}$$

The vented steam flow under this condition can be calculated as

$$\dot{m}_{soid} = Q_{id}\ \rho_{sat}(T_{wi}) , \tag{8}$$

where ρ_{sat} is the saturated steam density at the given temperature. Now the condensed steam at ideal conditions is

$$\dot{m}_{scid} = \dot{m}_{si} - \dot{m}_{soid} . \tag{9}$$

With $\varepsilon_w = 1$, the ideal (minimum) water flow rate required to condense this steam is

$$\dot{m}_{wid} = \dot{m}_{scid}\ h_{fg}/C_{pw}\ (T_{si} - T_{wi}) . \tag{10}$$

Correlating Variables

Now, a new variable, a liquid flow fraction ℓ defined as

$$\ell = \dot{m}_{wid}/\dot{m}_{wi} , \tag{11}$$

is formed. This variable ℓ can now be used to correlate the water effectiveness ε_w. It can be readily shown that, provided the vented steam flow is small compared with the inlet steam flow,

$$\ell \simeq \varepsilon_w . \tag{12}$$

To correlate ε_s, a function of vent rate and pressure loss, first a maximum exit steam temperature $T_{s\ max}$ is found by stipulating $\rho_{ii} = \rho_{io}$; i.e., inlet and outlet volumetric flow rate of the steam-gas mixture is the same,

$$\frac{P_c\ y_{ii}}{T_{si}} = \frac{[P_c - P_{sat}(T_{s\ max}) - \Delta p]}{T_{s\ max}} . \tag{13}$$

Now, defining two new variables ξ - a modified fractional steam effectiveness

$$\xi = \frac{T_{s\ max} - T_{so}}{T_{s\ max} - T_{wi}} , \tag{14}$$

and v - a modified volumetric vent fraction

$$v = \frac{\rho_{io} - \rho_{ii}}{\rho_{iid} - \rho_{ii}} , \tag{15}$$

it can be readily shown that when $v = o$, $\xi = o$ and when $v = 1$, $\xi = 1$. Further, ξ increases monotonically with increasing v.

The liquid and gas loadings L and G for the condenser packing are calculated as

$$L = \dot{m}_{wi}/A \tag{16}$$

and

$$G = (\dot{m}_{si} + \dot{m}_{ii})/A , \tag{17}$$

where A is the cross-sectional area of the condenser.

A pressure-loss coefficient based on the dynamic pressure of the inlet steam-gas mixture K defined as

$$K = 2\ \Delta p(\rho_{si} + \rho_{ii})/G^2 \ , \qquad (18)$$

is also calculated.

The experimental data for the seven packings are presented as plots of ε_w versus ℓ, ξ versus v, and K versus v.

The number of transfer units (NTU) for condensation is evaluated as

$$NTU = \int_{T_{wi}}^{T_{wo}} \frac{dT_w}{T_s - T_w} \ . \qquad (19)$$

To evaluate this integral, it is convenient to view the heat transfer process during condensation as a plot of condenser heat load versus a steam outlet temperature T_{so}, as shown in Fig. 3. This figure is generated for the following conditions:

$$T_{si} = 15^oC;\ T_{wi} = 5^oC;\ \varepsilon_w = 0.8;\ \varepsilon_s = 0.8;$$

$$\dot{m}_{wi} = 6.9\ kg/s;\ \dot{m}_{ii} = 2\ g/s \ .$$

The heat load curve is generated by assuming various values for T_{so} ranging from T_{wi} to T_{si}. The pressure loss in the condenser is assumed to be negligible for these calculations.

At an assumed $T_{so} = T_s$, the inert outlet concentration x_{io} and the outlet steam flow rate $\dot{m}_{so}$ are calculated. Therefore, the condensed steam flow is

$$\dot{m}_{sc} = \dot{m}_{si} - \dot{m}_{so} \qquad (20)$$

and the condenser heat load is

$$h = \dot{m}_{sc}\, h_{fg} \ . \qquad (21)$$

As the outlet steam temperature decreases from T_{si}, the heat load increases rapidly at first. With further decreases in T_{so}, the heat load levels off to a more or less constant value.

A similar calculation for the heat absorbed by the water stream is straight-forward,

$$h = \dot{m}_{wi} C_{pw}\ (T_{wo} - T_{wi}) \ , \qquad (22)$$

yielding a straight line.

As the water temperature rises from T_{wi} to T_{wo} because of increasing contact with the steam through its fall through the condenser, the steam temperature decreases from T_{si} at the bottom of the condenser to T_{so} at the top.

At any location within the condenser, the driving temperature differential for the heat transfer between the steam and water is

$$\Delta T = T_s - T_w \ . \qquad (23)$$

Note that at the low inert gas levels dealt with in this paper, ΔT is small at both the condenser inlet and exit, and reaches a maximum somewhere within the condenser area.

The NTU integral is obtained by integrating the inverse of this temperature difference by an adaptive quadrature routine QUANC8 (12).

A height of transfer unit (HTU) is obtained by dividing the overall height of the condenser gas-liquid contacting area by NTU as

$$HTU = l_c/NTU \qquad (24)$$

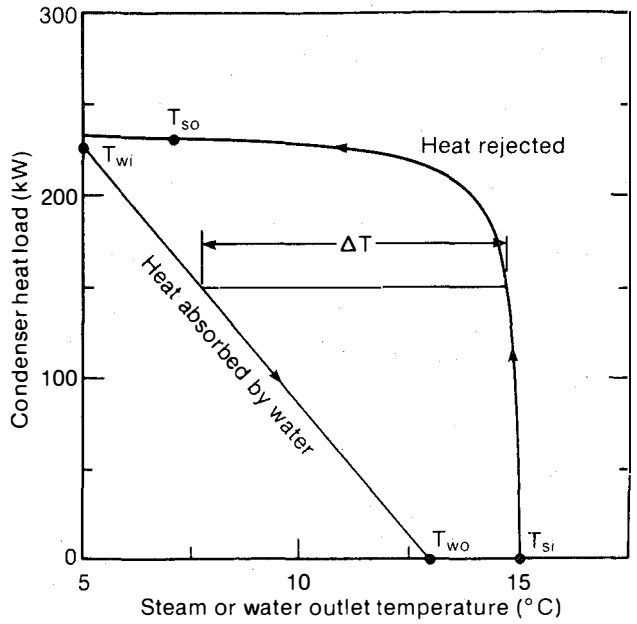

Fig. 3 An Operating Diagram for the Countercurrent Condenser.

EXPERIMENTAL RESULTS

A summary of the tested range of important condenser parameters is provided in Table 2. A total of 1003 data points are reported in this paper. Tests with seven different configurations include a steam inlet temperature range of 8.6° to 24.2°C, an inlet inert gas mass fraction of 0.15% to 10.2%, and an outlet inert gas mass fraction of 2% to 78%.

Water Effectiveness

The measured water effectiveness ε_w is plotted as a function of the liquid-flow fraction ℓ in Fig. 4. Data for all seven configurations is included in this figure. To improve clarity, only a shaded region over which the experimental data fell is shown. The water effectiveness appears to be primarily a function of the liquid flow fraction.

For $0.1<\ell<0.85$, ε_w data fall close to the line $\varepsilon_w = \ell$. Measured ε_w is, however, slightly smaller than ℓ by at most 3%.

For $0.85<\ell<1.2$, ε_w data deviate considerably from the line $\varepsilon_w = \ell$. In fact, ε_w increases from about 0.84 to 0.95, as ℓ increases from 0.85 to 1.0. The effectiveness then levels off at 0.95 with further increases in the fraction.

Scatter in the experimental measurements is quite small (±2% in the worst case), but is not self-evident from this figure.

Steam Effectiveness

The measured steam effectiveness ε_s is plotted as a modified fractional steam effectiveness ξ vs the vent fraction v for all the tested configurations in Fig. 5. Again, to improve clarity, only a shaded area over which the experimental data fell is shown in this figure. The measured ξ data fall along a diagonal line, increasing with v.

Two solid lines representing the theoretical variations of ξ with v at two steam inlet temperatures are also shown in this figure. At a steam inlet temperature T_{si} of 8°C, the theoretical line is almost a straight diagonal line beginning at the origin. At

Table 2. Condenser Parameters Test Range

Condenser Configuration	Water Inlet Temperature (°C)		Steam Inlet Temperature (°C)		Condenser Pressure (Pa)		Pressure Loss (Pa)		Inert Gas Inlet Mass Fraction (%)		Inert Gas Outlet Mass Fraction (%)		Vented Volumetric Flow (m^3/s)		Liquid Loading ($kg/s \cdot m^2$)		Gas Loading ($kg/s \cdot m^2$)		Measured Minimum HTU (m)	HTU (m) at $\ell = 1$	Total number of data points
	Min.	Max.	Min.	Max.	Min.	Max.	Min.	Max.	Min.	Max.	Min.	Max.	Min.	Max.	Min.	Max.	Min.	Max.			
#1	4.23	6.35	8.93	17.43	1150	2030	12	530	0.15	9.40	8.7	65	0.06	0.22	48	80	0.18	0.62	0.49	0.28	105
#2	3.93	6.91	10.78	20.86	1300	2500	128	780	0.33	2.75	14.1	64	0.2	0.23	28	46	0.18	0.42	0.49	0.25	45
#3	4.19	5.79	10.35	22.70	1260	2800	72	850	0.27	2.50	11.3	61	0.20	0.26	22	44	0.16	0.49	0.25	0.25	59
#4	4.76	5.65	10.85	24.22	1300	3070	15	70	0.38	2.40	12.0	37	0.21	0.26	29	30	0.15	0.37	0.54	0.25	20
#5	4.58	5.87	9.13	20.46	1160	2440	4	60	0.26	2.40	3.6	69	0.03	0.24	22	47	0.16	0.45	0.28	0.30	239
#6	4.56	5.68	8.63	21.15	1130	2540	2	40	0.30	2.45	3.2	73	0.05	0.22	22	47	0.15	0.43	0.27	0.28	257
#7	4.64	5.54	9.92	21.91	1220	2780	2	65	0.28	10.20	1.7	78	0.05	0.56	21	45	0.15	0.51	0.27	0.28	278

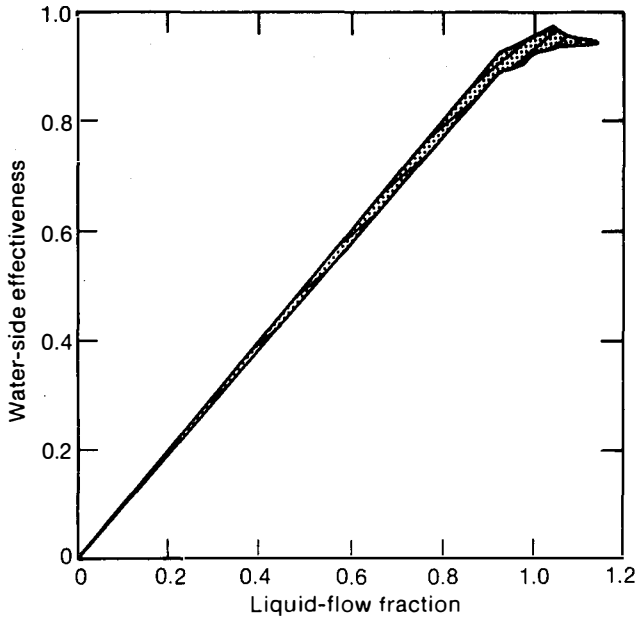

Fig. 4 Measured Water Effectiveness ε_w vs. the Liquid Flow Fraction ℓ.

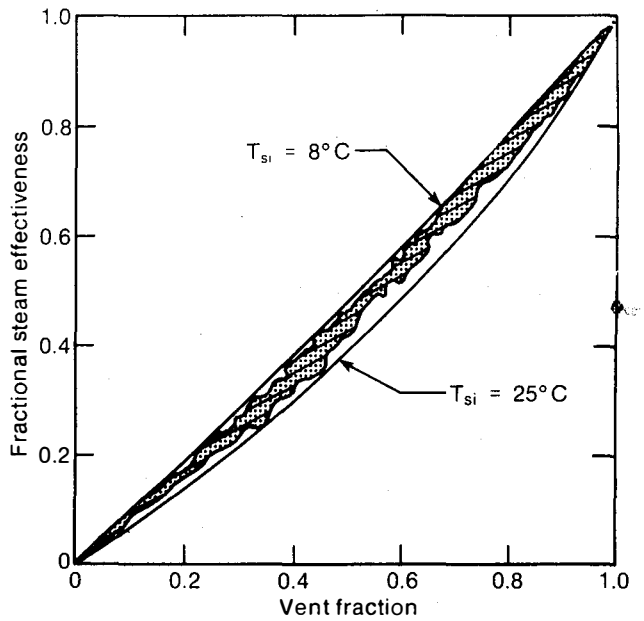

Fig. 5 Measured Fractional Steam Effectiveness ξ vs. the Vent Fraction v.

T_{si} = 25°C, because of the nonlinear variation of steam saturation pressure with temperature, the theoretical variation is curved and falls below the diagonal. These two curves bound the ξ data variation for all the measurements.

These data indicate that ξ is primarily a function of v and T_{si}; i.e., $\xi = \xi\ (v, T_{si})$. However, note that by definition ξ and v are dependent upon the condenser pressure loss Δp and the inert gas content in steam x_{ii}.

Performance Maps

At a given $\dot{m}_{si}$, x_{ii}, and T_{wi}, the lowest achievable condenser pressure P_c may be limited by the heat-transfer rate or by the exhaust capacity or both, for a particular condenser configuration.

The heat-transfer rate (or the condensation rate) is a function of the condenser configuration, the available interfacial area for condensation, the driving temperature potential, and the pressure loss through the condenser. The limitation posed by the exhaust system is a function of the condenser pressure, the pressure-loss, and heat-transfer characteristics of the condenser. In fact, the limitations due to the heat-transfer rate and the exhaust capacity are interrelated and cannot be estimated prior to testing.

One of the goals of this study is to map out the operating characteristics of the tested configurations and identify these limitations. This was accomplished by testing a configuration over a wide range of test parameters to include operating conditions where these limitations did and did not occur.

A typical performance map for configuration 6 is

shown in Fig. 6 as a plot of measured ε_w vs. ε_s. The experimental data cover a wide range of ε_s, ε_w, and other condenser test parameters (see Table 2). Also shown in this figure is the maximum potential performance for this configuration as an envelope of the data representing the maximum ε_s for a given ε_w or vice versa. Along this envelope, as ε_s increases from 0.1 to 0.8, ε_w decreases only slightly from 0.95 to nearly 0.86. With further increases in ε_s, ε_w decreases sharply to nearly 0.4.

The limitations on the maximum potential performance of the condenser can now be identified as follows: At low values of ε_s ($0.1<\varepsilon_s<0.7$), since ε_w remains nearly constant and since $\varepsilon_w \simeq 1$, increasing the coolant flow rate results in a corresponding reduction in P_c. At this point, the condenser pressure is a function of the condensation rate, which, in turn, is related to the liquid flow rate within the condenser. On the contrary, any changes in ε_s in this region, correspond to changes in exhaust capacity, but do not alter the condenser pressure.

At high values of ε_s (>0.9), ε_w decreases rapidly with increasing ε_s. In this region, any increase in liquid flow rate is accompanied by a corresponding reduction in ε_w, causing no changes in P_c. P_c is limited by the exhaust capacity. Since ε_s is nearly constant, increasing the exhaust capacity will result in lowering P_c.

There exists a region over which both the condensation rate and the exhaust capacity limit the condenser performance. This region corresponds to $0.7<\varepsilon_s<0.9$. At all other experimental conditions when the data fall within the envelope, neither of these limitations occur.

A precise value of ε_s on the envelope at which the condenser pressure changes from being limited by the condensation rate to being limited by the exhaust capacity is difficult to define. A method to estimate this transition is to identify an ε_s value at which the product $\varepsilon_s \times \varepsilon_w$ attains a maximum. This method identifies the transition point for all the configurations.

Similar maximum potential performance envelopes for all the tested configurations are shown in Fig. 7. Transition values of ε_s above which the exhaust capacity limits the condenser pressure are included. At a given ε_w we obtained increasingly higher ε_s values for configurations in the following order: 4, 3, and 5; 1 and 2; and 6 and 7.

Among all the configurations tested, configurations 6 and 7 yielded the highest overall condenser performance because of their large available surface area per unit volume (approximately 98 and 138 m^2/m^3, respectively) and low pressure-loss coefficients (approximately 10 to 20, see section on pressure loss). We observed little difference between the performances of these two configurations.

Configurations 3 and 5 yielded a somewhat lower performance. Configuration 5, despite its low pressure-loss coefficient, perhaps did not provide as much contact area as configurations 6 and 7. Whereas configuration 3, consisting of two pairs of disc-and-donut baffles, yielded rather large pressure-loss coefficients.

Configurations 1 and 2 yielded similar performances. Note that for either of these configurations, the vacuum capacity limited the condenser operation at all test conditions. Configuration 1, despite its low pressure-loss coefficient (of nearly 30 to 40), was of a smaller diameter and cross-sectional area than all others and, hence, was tested at liquid and gas loadings nearly twice that for all others. Thus, the associated larger vapor pressure losses limited the test conditions to regions where the vacuum

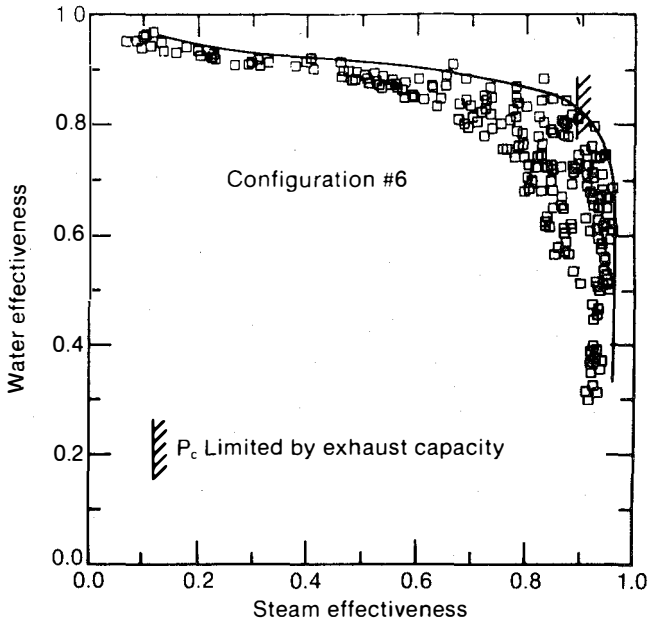

Fig. 6 Performance Map of Configuration 6 Plotted as Water Effectiveness versus Steam Effectiveness.

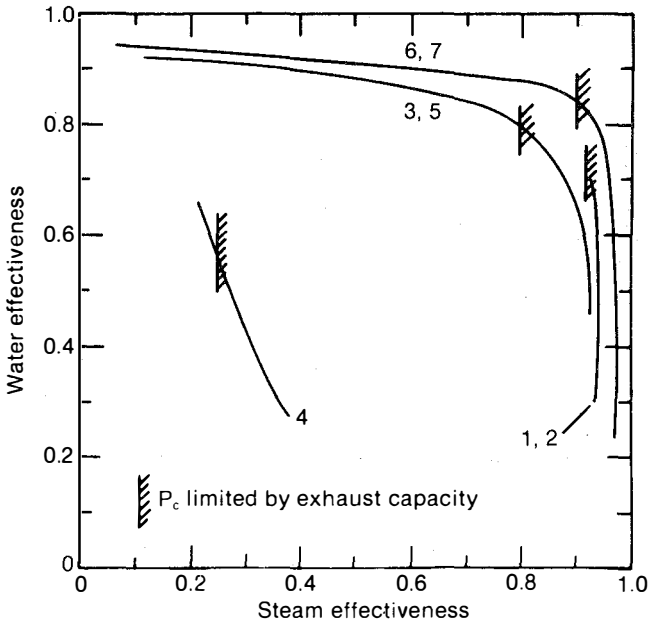

Fig. 7 Maximum Performance Envelopes for the Various Tested Configurations.

capacity restricted the condenser operation. A high pressure-loss coefficient for configuration 2 posed similar restrictions in this condenser operation (despite its lower liquid and gas loading levels).

Configuration 4, consisting of a single pair of disc-and-donut baffles, yielded the lowest performance among all. However, since its pressure-loss coefficient is low (nearly 10 to 20), the performance reduction is caused by inadequate contact between steam and water.

Pressure Loss

The pressure loss through the condenser is a function of the configuration, its liquid, and gas loading. For the tested configurations the pressure-loss data is presented in terms of a pressure-loss coefficient K defined in eq. (18).

The pressure-loss coefficient is plotted as a function of the vent fraction in Figs. 8 and 9. Fig. 8 includes the loss coefficients for the low-loss configurations (all except 2 and 3). The pressure-loss data exhibit considerably large scatter. This scatter, perhaps, arises from varied liquid loadings and a continuously decreasing gas loading through the condenser. Attempts to correlate the data with liquid loading did not reduce this scatter. Despite the large scatter, the data does provide bases for obtaining order of magnitude estimates for the pressure-loss coefficient K. From the measurements, approximate estimates of K for the five configurations presented in Fig. 8, are 40, 5, 10, 10, and 10, for configurations No. 1, 4, 5, 6, and 7, respectively.

Configurations 2 and 3 yielded considerably larger pressure losses because of the additional obstruction introduced by the added set of baffles. These data are included in Fig. 9. Estimates of K for these configurations are about 80 and 100, respectively. Uncertainty in these K estimates is about ±50%, based on the data scatter.

It should be emphasized that these K estimates are for the tested configurations only. Caution must be exercised in using these K values to estimate losses for other geometries. The main obstacle in assessing presssure losses is that the gas loading through the condenser varies continuously and rapidly. The loss coefficients presented are based on an inlet gas loading. Because of condensation on the liquid draining from the packings and on the water pool, the gas loading at the entry of the packing may be considerably smaller.

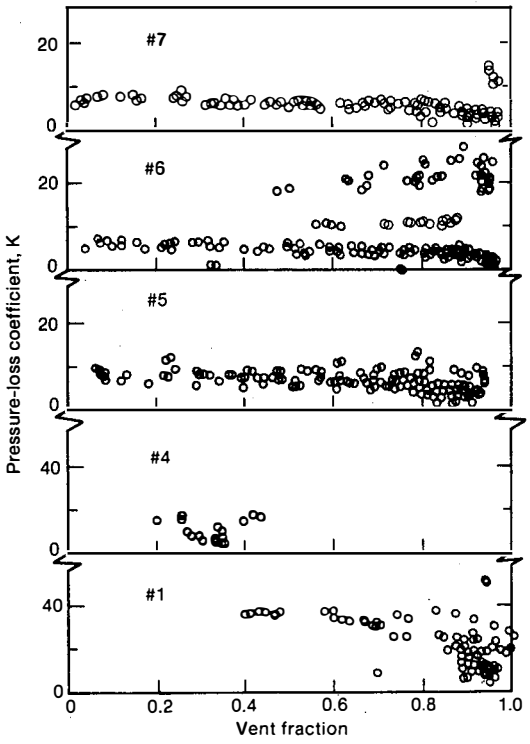

Fig. 8 Pressure-Loss Coefficient K vs. the Vent Fraction v for Condenser Configurations 1, 4, 5, 6, and 7.

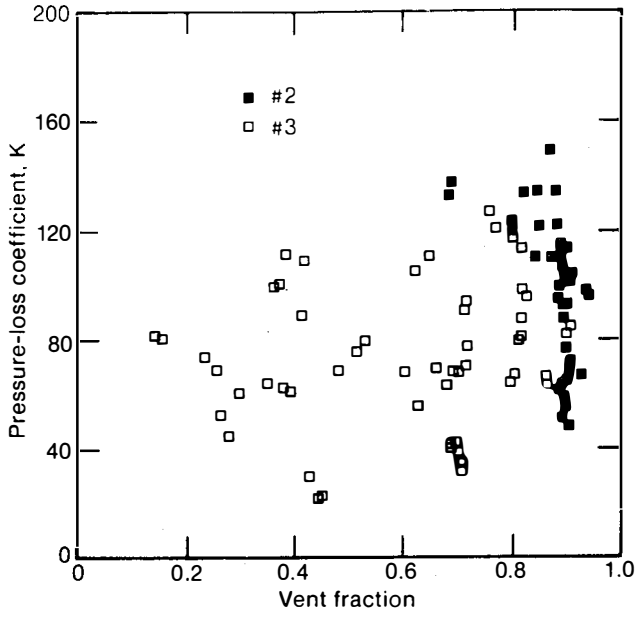

Fig. 9 Pressure-Loss Coefficient K vs. the Vent Fraction v for Condenser Configurations 2 and 3.

Height of Transfer Unit (HTU)

For test conditions when the condenser operation was governed by the condensation rate, HTU was evaluated for various configurations. A plot of HTU variation with the liquid fraction is shown in Fig. 10. Typically, HTU decreases with increasing ℓ, being almost inversely proportional to ℓ for ℓ values of up to unity. For $\ell > 1$, HTU remains more or less constant. Minimum values of HTU obtained for the various configurations range from 0.25 to 0.3 m.

For the configurations 6 and 7, the HTU data was fitted to a correlation of the form of eq. (1) in a least-square sense. Since only two H values were tested, the dependence of St on H was fixed at a power of -0.67. For lack of contrary data, the wetted-to-total area ratio was taken to be unity. The resulting fit yielded the following relation between St, Ja, C, and H:

$$St = 0.091\ Ja^{1.55} C^{-0.5} H^{-0.67} \qquad (25)$$

This equation predicts the HTU with a standard deviation of about 9%.

OTEC APPLICATIONS

To illustrate how the selection of a condenser subsystem performance may affect the design of an open-cycle OTEC plant, two contour maps indicating the relative variations of the subsystem parasitic power and cost as functions of the condenser water and steam effectiveness for a typical 5-MW_e gross floating plant are shown in Figs. 11 and 12.

These figures were generated with the following assumptions:

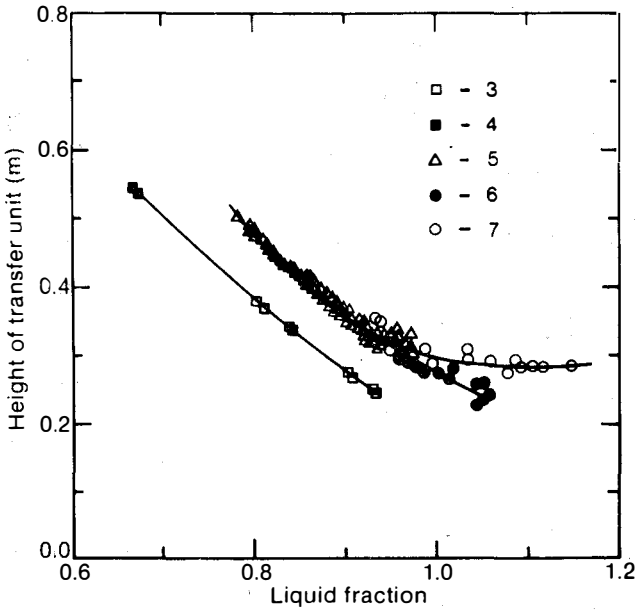

Fig. 10 Measured Height of Transfer Unit versus Liquid Flow Fraction for Various Configurations.

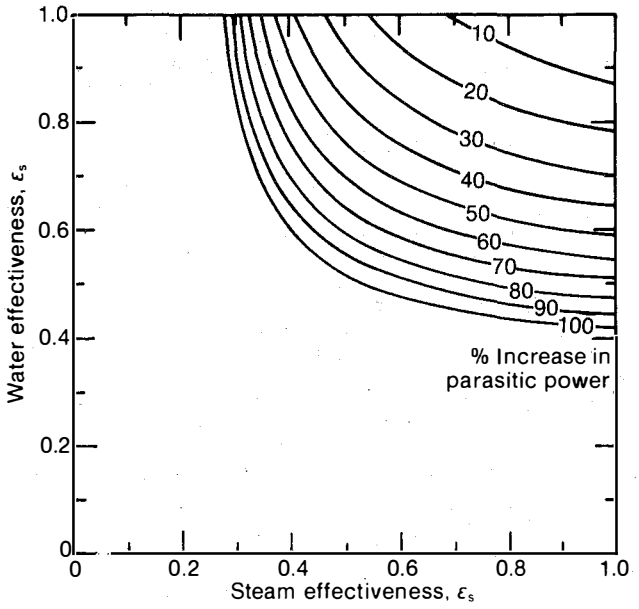

Fig. 11 Relative Increase in Parasitic Power of Condenser Subsystem as a Function of Water and Steam Effectiveness for a 5-MW_e Floating Open-Cycle OTEC System.

Cold water pipe length = 1000 m
Cold water pipe cost = 2000/(length x diameter) $/m^2
Cold water loop head loss = 3.5 m
No. of stages in vacuum exhaust compressor train = 4
Cold water inlet temperature = 5°C
Condenser vapor pressure loss = 100 Pa
Price of electricity = 11¢/kWh
Fixed charge rate on capital cost = 0.06

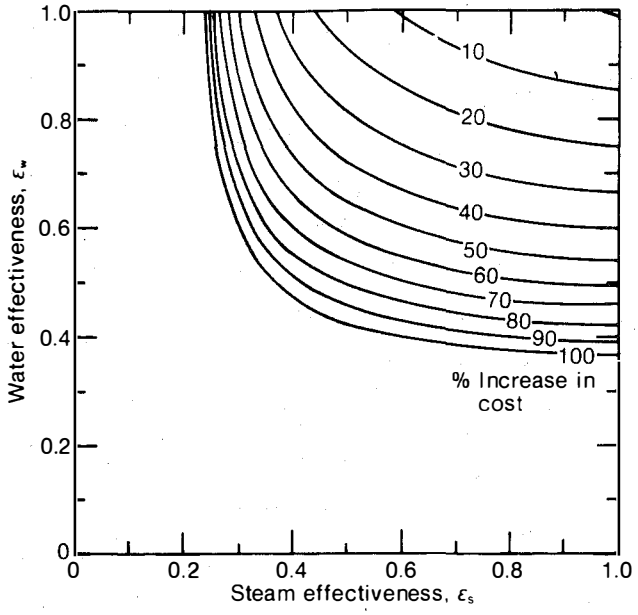

Fig. 12 Relative Increase in Cost of Condenser Subsystem as a Function of Water and Steam Effectiveness for a 5-MW_e Floating Open-Cycle OTEC System.

Additional assumptions relevent to these figures include: ideal water and gas exhaust pumps with efficiencies of unity and interstage-coolers with gas exhaust temperatures of 5°C. The capital cost associated with the water pump and gas exhaust system were taken from cost models for OTEC systems provided in Ref. 13.

Figure 11 illustrates the relative increase in parasitic power as a function of condenser effectiveness. Of course, the minimum parasitic power occurs at ε_s and ε_w equal to unity. For ε_s in the range of 0.8 to 1.0, the increase in parasitic power is inversely proportional to ε_w, reaching 100% at ε_w of 0.4. For ε_s values of less than 0.8, the parasitic power is affected by both ε_s and ε_w. Decreases in either ε_s or ε_w result in increased parasitic power.

Figure 12, indicating the increase in relative cost of the condenser subsystem as a function of the condenser effectiveness, is essentially similar in features to Fig. 11.

Based on these two figures and to limit the relative cost or power increases to less than 20%, the water effectiveness must be greater than about 0.85 and the steam effectiveness greater than about 0.60 for the particular set of adopted assumptions. These relative power and cost performances vary with the particular design of a plant for a specific purpose and need. The choice of a condenser subsystem again depends on the application.

CONCLUDING REMARKS

Seven different countercurrent condenser configurations were tested at experimental conditions relevant to open-cycle OTEC systems. Relative performances of the configurations are identified using maximum potential envelopes in a map of water effectiveness vs. steam effectiveness. We also identified experimental conditions when the exhaust capacity of the vacuum system limited the condenser operation. For

conditions when the condensation rate was limiting, the measured HTUs are presented as a function of a liquid flow fraction. For all tested configurations the water effectiveness is correlated as a function of the liquid flow fraction and the steam effectiveness as a function of a vent fraction. Identified pressure-loss coefficients for the tested configurations varied widely from nearly five to a maximum of 100. For the majority of the condenser configurations acceptable liquid loading for direct-contact condensation are in the range of 20 to 40 kg/s m^2. However, limitations on the gas loading depend on an allowable maximum vapor pressure loss through the condenser. Performance indexes as relative increases in parasitic power and cost for a typical OTEC application provide bases for evaluating various condenser configuration options.

ACKNOWLEDGMENTS

We would like to express our gratitude to the U.S. Department of Energy, Ocean Energy Technology Division, for their support in carrying out this work. The Munter's Corporation is acknowledged for providing samples of surface media for use as test articles.

REFERENCES

1. Bharathan, D., Kreith, F., and Owens, W. L., "An Overview of Heat and Mass Transfer in Open-Cycle OTEC Systems," Proceedings of the ASME/JSME Thermal Engineering Joint Conference, Mori, Y. and Yang, W. J., eds., March 1983, pp. 301-314.

2. Sideman, S. and Moalem-Maron, D., "Direct Contact Condensation," Advances in Heat Transfer, Hartnett, J. P. and Irvine, Jr., T. F., eds., Vol. 15, Academic Press, New York, 1982, pp. 227-281.

3. Wilke, C. R., Cheng, C. T., Ledesma, V. L., and Porter, J. W., "Direct Contact Heat Transfer for Seawater Evaporation," Chemical Engineering Progress, Vol. 59, No. 12, December 1963, pp. 69-75.

4. Cheng, C. T., "Direct-Contact Condensation in a Packed Tower," Masters Thesis, Department of Chemical Engineering, University of California, Berkeley, 1963.

5. Thomas, K. D., Jacobs, H. R., and Boehm, R. F., "Direct Contact Condensation of Immiscible Fluids in Packed Beds," Condensation Heat Transfer, American Society of Mechanical Engineers, New York, August 1979, pp. 103-110.

6. Fair, J. R., "Design of Direct-Contact Gas Coolers," Petroleum and Chemical Engineer, Vol. 2, August 1961, pp. 203-210.

7. Fair, J. R., "Process Heat Transfer by Direct Fluid-Phase Contact," AIChE Symposium Series on Process Heat Transfer, 12th National Heat Transfer Conference, Tulsa, Oklahoma, Vol. 68, No. 118, August 1971, pp. 1-11.

8. Fair, J. R., "Designing Direct-Contact Coolers/Condensers," Chemical Engineering, Vol. 2, June 1972, pp. 91-100.

9. Sherwood, T. K., Shipley, G. H., and Holloway, F. A. L., "Floating Velocities in Packed Columns," Industrial Engineering Chemistry, Vol. 30, 1938, pp. 765-769.

10. Schweitzer, P. A., ed., Handbook of Separation Techniques for Chemical Engineers, McGraw-Hill, New York, 1979.

11. Green, H. J., Olson, D. A., Bharathan, D., and Johnson, D. H., "Measured Performance of Falling Jet Flash Evaporators," SERI/TP-631-1270, Solar Energy Research Institute, Golden, CO, June 1981.

12. Forsythe, G. E., Malcolm, M. A., and Moler, C. B., Computer Methods for Mathematical Computations, Prentice-Hall, Englewood Cliffs, N.J., 1977, pp. 97-105.

13. Hall, M. H., Hutchings, B. J., Patel, B. R., Sam, R. G., Stacy, W. D., and Valenzuela, J. A., "Thermo-Economic Analysis of Open-Cycle OTEC Plants," to be presented at the ASME Winter Annual Meeting, New Orleans, Dec. 9-14, 1984.